**Showcasing research from Professor Yun-Hong Zhang's laboratory, School of Chemistry and Chemical Engineering, Beijing Institute of Technology, Beijing, China.**

Directly measuring Fe(III)-catalyzed SO$_2$ oxidation rate in single optically levitated droplets

We directly measure the kinetics of Fe(III)-catalyzed SO$_2$ oxidation at the surface of a single droplet trapped by optical tweezers. The Fe(III)-catalyzed SO$_2$ reactive uptake coefficient is 2 or 3 orders higher than that of the auto-oxidization without TMI. The reaction rate decreases by up to a decade when the Fe(III)/S(VI) coexisting time increases, owing to a complexation between Fe(III) and S(VI).
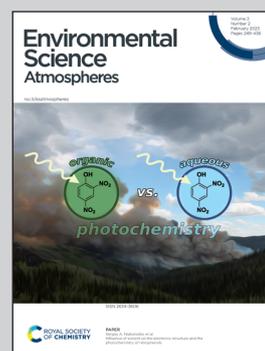
ROYAL SOCIETY
OF CHEMISTRY

rsc.li/esatmospheres

Check for updates

Directly measuring Fe(III)-catalyzed SO$_2$ oxidation rate in single optically levitated droplets†

Xue Cao, Zhe Chen, Yu-Xin Liu, Xin-Bo Jing, Lin-Fang Li, Pai Liu* and Yun-Hong Zhang [ID] *

Sulfate aerosols are produced in China's winter haze at an unresolved rapid rate. Such fast kinetics may arise from a heterogeneous SO$_2$ conversion in urban aerosols, which differs significantly from the aqueous S(IV) oxidation in bulk solutions. Given the uniqueness of aerosols as a multiphase reactor, it is preferable to measure the heterogeneous SO$_2$ conversion rate *in situ*, ideally in levitated microdroplets. Here, we directly measure the Fe(III)-catalyzed SO$_2$ conversion in single microdroplets trapped and levitated with a gradient-force aerosol optical tweezer. The sulfate formation rate was inferred from the droplet's growth rate driven by the heterogeneous reaction. Our results show that the Fe(III)-catalyzed SO$_2$ conversion in aerosols is 2 to 3 decades faster than that determined in bulk solutions. The SO$_2$ reactive uptake coefficient at pH ~5.0 and 298 K is on the order of 10^{-4} to 10^{-3}. The reaction rate scales with droplet surface area, indicating that the major reaction location is the air–water interface. This interfacial reaction is further corroborated by a positive kinetic salt effect, a trait of the interaction between ions and the neutral molecules, such as Fe(III) ions and SO$_2$ molecules. The reaction rate decreases by up to a decade, as the Fe(III)/S(VI) coexisting time increases, possibly owing to a complexation between Fe(III) and S(VI) ions.

Environmental significance

Sulfate is a major secondary inorganic component of atmospheric particulate matter, and its production is closely related to urban haze formation. Sulfate can be produced rapidly *via* a heterogeneous process, in which SO$_2$ molecules are directly converted at the aerosol surface, catalyzed by the transition metal ions. In this study, we directly measure the kinetics of Fe(III)-catalyzed SO$_2$ oxidation at the aerosol surface. The kinetic effects of SO$_2$ concentration, total Fe(III) molar fraction, ambient humidity, and hours of S(VI)/Fe(III) coexistence are investigated. We emphasize that the SO$_2$ conversion rate in incipient aerosols and in aged ones can differ by nearly a decade, which should be incorporated in the air-quality models.

1 Introduction

The rapid formation of sulfate aerosols is the chemical driver of the severe winter haze events in China, exerting tremendous negative impacts on social economy and public health.[1–4] During the past decade, SO$_2$ emission in China's urban area has been effectively controlled: The annual average SO$_2$ concentration decreased from 9.1 ppb in 2013 to 1.7 ppb in 2018.[5] Yet, during the same period, sulfate aerosol concentration in polluted air only decreased moderately, from 19.2 to 12.1 μg m^{-3}.[6] And severe air pollution events still occurred in winter seasons.[4,7,8] To further contain secondary sulfate pollutants, we need to thoroughly understand the mechanisms and kinetics of SO$_2$ conversion in polluted air.

Institute of Chemical Physics, School of Chemistry and Chemical Engineering, Beijing Institute of Technology, 100081, Beijing, China. E-mail: pliu@bit.edu.cn; yhz@bit.edu.cn

Per the traditional view, SO$_2$ in the gas phase is oxidized by OH radicals[9] and stable Criegee intermediates.[10] Aqueous reaction pathways include the oxidation of S(IV) by O$_3$, O$_2$ (catalyzed by transition metal ions, TMI), and H$_2$O$_2$ dissolved in cloud and fog droplets.[11,12] But these mechanisms cannot explain the rapid sulfate PM$_{2.5}$ formation in the north China plain (NCP). The sulfate PM$_{2.5}$ concentration simulated with air quality models[13] were 3–4 times lower than that measured in the atmosphere. This gap has motivated many research efforts to discover the hitherto unidentified sulfate sources in polluted environments:[11,14–22] New aqueous SO$_2$ conversion mechanisms have been identified, and the kinetics of existing mechanisms have been updated.

The significance of aqueous SO$_2$ conversion, however, was questioned in recent kinetic studies.[1,23] The concern partly arises from a reaction space constraint.[1,23] The volume of aerosol water in polluted air is several decades smaller than that of clouds, and such small aerosol water volume precludes large-scale sulfate formation *via* aqueous routes.[1] Instead, interfacial reactions – a direct conversion of SO$_2$ molecules at the

aerosol surface – can exploit the large surface area of micro-droplets and thereby produce sulfate rapidly. Wang et al.[1] reported that the Mn(II)-catalyzed SO$_2$ oxidation at the aerosol surface is two decades faster than that in bulk solutions. A subsequent air-quality model simulation[23] showed that this Mn(II)-catalyzed interfacial reaction accounts for 92.5% of the sulfate in the NCP haze events. These lab studies and model simulations indicate that the dominating sulfate formation mechanism in polluted air is interfacial SO$_2$ oxidation catalyzed by TMI, primarily by Mn(II) ions.[1,23]

The recent studies emphasized the significance of TMI-catalyzed SO$_2$ oxidation at aerosol surface,[1,23] but some knowledge gaps still exist in our understanding of this reaction route. For example, the reaction kinetics of Fe(III)-catalyzed SO$_2$ oxidation remain unconstrained. In traditional solution chemistry, both Fe(III) and Mn(II) ions were known for their catalytic effects expediting the aqueous S(IV) oxidation.[24] And when Fe(III) and Mn(II) coexist, a synergistic effect[25] leads to a reaction rate faster than the summation of the rates of the reactions catalyzed by individual Fe(III) or Mn(II). But recent chamber studies[1,16] showed that the Fe(III)-catalyzed reaction did not produce sulfate aerosols at a rate as rapid as the Mn(II)-catalyzed one. Zhang et al.[16] reported that the Fe(III)-catalyzed reaction is immeasurably slow; When both Fe(III) and Mn(II) were added, very limited synergist effects were observed. Wang et al.[1] also reported that adding Fe(III) ions did not accelerate sulfate formation; When Fe(III) and Mn(II) coexist, an increase in Fe(III) mixing fraction did not cause any increase in reaction rate. Another recent study by Angle et al.[17] showed that the TMI-catalyzed oxidation of aqueous S(IV) is faster in microdroplets than in bulk solution, possibly owing to a rate-enhancing effect of the air–water interface. Such a rate enhancement was observed for both the Mn(II)-catalyzed reactions and the Fe(III)-catalyzed ones.[17] It remains unclear why the Fe(III) ions lose their capability when the reaction occurs at the aerosol surface.

These knowledge gaps have motivated the present study. Here, we directly measured the rate of Fe(III)-catalyzed SO$_2$ oxidation in single (NH$_4$)$_2$SO$_4$ droplets levitated by an aerosol optical tweezer (AOT).[17,26] The AOT utilizes optical gradient force to steadily trap a single droplet,[27,28] allowing us to measure the reaction rate in it with Raman spectroscopy.[17,26] Measuring kinetics in a single levitated droplet has the following advantages. First, when the target being measured is a single droplet, it is much easier to manipulate the droplet properties (size, composition, and ionic strength) and ambient conditions (gas concentration, humidity).[11,17,26] Second, when a droplet is levitated at the optical trap, the backscattered Raman light can be exploited for an in situ kinetic measurement[17,26] during reactions. Third, a single droplet is an optical resonant cavity, and the cavity-enhanced Raman spectra (CERS) reveal the reaction-induced hygroscopic growth of the droplets with a nanometer precision.[27,28] This one-nanometer droplet growth can then be used to infer the sulfate production at a 10^{-14} mol precision.[26]

In the following, we first describe the experimental setup of AOT that facilitated measuring reaction kinetics in levitated droplets. This is followed by a recap on how to infer reaction rate from droplets' hygroscopic growth. Next, we discuss the

reaction rate as a function of SO$_2$ concentration, droplet size, Fe(III) concentration, ionic strength, and aging time. We conclude with the atmospheric implication of our findings.

2 Methods

2.1 Aerosol optical tweezer

The AOT system is the same one used in our previous study,[26] and one may refer to the ESI† of that paper for details of AOT schematics and gas-flow arrangements. Here, we only provide a brief recap on the key specifications of the apparatus. The optical trap was constructed with a 532 nm Gaussian beam tightly focused inside a 6 mL sample cell. Specifically, this beam was focused with a 100× oil immersion objective scope (Olympus UIS2 PlanCN) with a numerical aperture of 1.25. Similar to the design by Reid and coworkers,[27] our system uses the 532 nm beam, which constructs the optical trap, to serve as the incident light for Raman scattering. When a single aerosol droplet was trapped and levitated, the backscattered Raman signal was captured with a spectrometer (Zolix Ominc λ-500, 1200 grooves per mm grating) with a time resolution of one frame per second.

2.2 Aerosol generation

Aerosols were generated by nebulizing standard solutes comprising a mixture of ammonium sulfate (AS, (NH$_4$)$_2$SO$_4$), ammonium bisulfate (ABS, NH$_4$HSO$_4$), and iron sulfate (IS, Fe$_2$(SO$_4$)$_3$). These chemicals were purchased from Sinopharm Chemical Reagent Co. (analytical reagents, purity ≥ 99.0%) without further purification. The molar ratio of AS and ABS was either 1 : 1 or 1 : 0; the molar fraction of IS was fixed at 0.001, 0.01, or 0.1%. One may refer to Table S1 in ESI† for the initial droplet compositions. Ultrapure water (18.2 MΩ cm, Barnstead Easypure II) was used to prepare the solution. The ultrasonic nebulizer was produced by Yuyue (402AI model).

2.3 Aerosol pH and ionic strength

Droplet pH was maintained at ∼5.0 by dissolving 8.00 ppm NH$_3$ gas into the droplet water comprising a mixture of AS and IS (or AS/ABS and IS). The ionic strength (I) was adjusted between ca. 15 and 36 mol kg^{-1} by changing the ambient relative humidity (RH) condition between 80% and 60%. The variation of RH during an experiment was maintained within ±1%. The values of droplet initial pH and I were computed with E-AIM model III,[29] per:

$$pH = -\log(\gamma_{H^+} m_{H^+}) \tag{1}$$

and

$$I = \frac{1}{2} \sum_i m_i \times z_i^2. \tag{2}$$

Here, γ_{H^+} and m_{H^+} respectively denote proton activity coefficient and molality; m_i and z_i respectively denote the molality and charge number of major ions in the droplet. These parameters at initial were regarded as representative to the droplet

© 2023 The Author(s). Published by the Royal Society of Chemistry

Environ. Sci.: Atmos., 2023, **3**, 298–304 | **299**

undergoing reaction. These parameters are tabulated in Table S1.† Note that the concentration of reactant gases was estimated with their dilution ratio. This technique is the same as that in our previous publication.[26]

2.4 Measuring reaction rate

When RH is fixed, the sulfate solute molarity, [S(VI)], is also a constant, owing to an equilibrium of water partition. At such an equilibrium condition, an increasing sulfate mass inside the droplet will cause an increasing droplet volume. In other words, converting SO_2 to sulfate inside a droplet will induce a hygroscopic growth of the droplet. Such reaction-induced droplet growth facilitates us to measure the reaction rate precisely, if we can measure the droplet size precisely, for example:

$$R_{S(VI)} = \frac{dS(VI)}{dt} = \frac{[S(VI)] \times 4\pi r_0^2 dr}{dt} \quad (3)$$

Here, $R_{S(VI)}$ is the reaction rate in mol s^{-1}; r is droplet radius, subscript zero indicates the initial state, and t is time. The droplet size during the reaction, $r(t)$, was inferred from the whispering gallery mode wavelength λ_{WGM} per the Mie scattering calculation[28] established by Preston and Reid (refer to ESI Fig. S1† for typical droplet growth data). It is also implicitly assumed in eqn (3) that the curvature effect of the droplet surface is insignificant. Such an assumption requires that the increase in droplet radius during the reaction is negligible when compared with the initial radius. In the experiments, we guaranteed that the increase in r is always less than 5% of r_0. The reactant SO_2 concentration ranged between 25 and 10^3 ppb. Each kinetic measurement was conducted at fixed RH conditions (60, 70, or 80%). The O_2 in the background air served as the oxidizer.

3 Results and discussion

3.1 Influence of SO_2 concentration

We first discuss the kinetic effect of SO_2 concentration. In these experiments, the droplet pH was maintained at ~5.0; the ambient RH, at ~60%; Fe(III) molar fraction, 0.01%. SO_2 concentration varied between 25 and 10^3 ppb. Fig. 1 plots the reaction rate $R_{S(IV)}$ as a function of SO_2 concentration. Note that the unit of $R_{S(IV)}$ here is mole of sulfate produced in a unit time per a single droplet. The trends in Fig. 1 show that the sulfate formation rate correlates positively with SO_2 concentration. Quantitatively, we show that a linear fitting (red line in Fig. 1) describes the data best, indicating that the reaction rate is first order in SO_2. This observation agrees with our knowledge of the Fe(III)-catalyzed SO_2 conversion.[30]

3.2 The location of heterogeneous reaction

The size dependence of reaction rate provides us insight on the location of heterogeneous reactions.[26] For example, if SO_2 are first dissolved in aerosol water and the S(IV) are oxidized homogeneously therein, the reaction rate will be proportional to droplet volume, $R_{S(VI)} \propto r_0^3$; if the SO_2 are directly converted at the droplet surface, the reaction rate will be proportional to
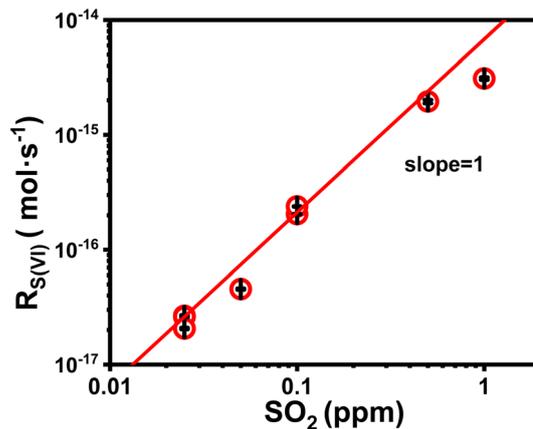

Fig. 1 The formation rate of sulfate inside a single levitated droplet, $R_{S(vi)}$, as a function of SO_2 concentration. The droplets were seeded with AS and IS mixture. The molar fraction of Fe(III) is 0.01%. Ambient RH was about 60%. The droplet pH was buffered at *ca.* 5.0 by dissolving an 8 ppm NH_3 into droplet water. The solid line represents a linear fitting on the dataset. Error bars arose from the uncertainty in determining dr/dt from the $r(t)$ data. The values of error stemmed from the 95% confidence interval of dr/dt values.

droplet surface area, $R_{S(vi)} \propto r_0^2$. We evaluated these scaling laws by using the droplet growth rate, dr/dt, which was measured directly during reactions. Eqn (3) indicates that dr/dt $\propto R_{S(vi)} \times r_0^{-2}$ holds for short-range droplet growth driven by sulfate formation. Then, the kinetic scaling laws can be reduced to dr/dt $\propto r_0$ for aqueous reaction, and to dr/dt = constant for the interfacial reaction.

Fig. 2 shows the dr/dt of droplets within two size bins: the smaller droplets around 4.5 μm radii, and the larger ones around 7.0 μm radii. The pH of these droplets was maintained at ~5.0; the SO_2 concentration, at 25 ppb; Fe(III) molar fraction, at 0.01%; RH, at ~60%. Inside these two size bins, we repeatedly
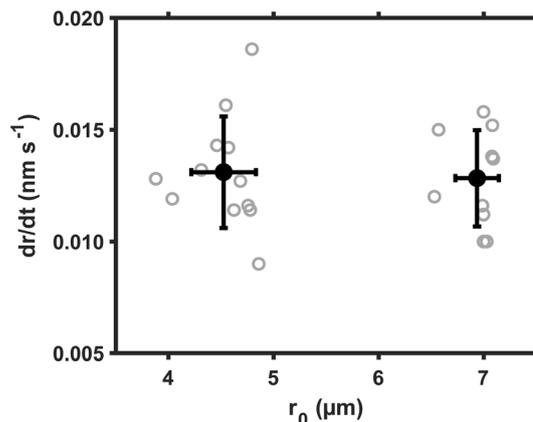

Fig. 2 Droplet growth rate during reaction, dr/dt, as a function of droplet initial radius, r_0. The ambient RH conditions were 60%; the SO_2 concentration, at 25 ppb; the droplet pH, at ~5.0. Gray circles represent the original dr/dt data; Black circles represent the mean values of dr/dt and r_0 for each cluster of data. Error bars represent on standard deviation.

300 | *Environ. Sci.: Atmos.*, 2023, **3**, 298–304

© 2023 The Author(s). Published by the Royal Society of Chemistry

Paper

measured dr/dt more than ten times (see the gray circles). Then we calculated the mean values for dr/dt and r_0, as well as their one standard deviation (black circles and error bars). Despite the fluctuation, the mean dr/dt values for droplets inside each size bin are clearly independent of the corresponding mean r_0 values. (The mean dr/dt was 0.0131 ± 0.002 nm s^{-1} and 0.0128 ± 0.002 nm s^{-1}, respectively, when the mean r_0 was 4.525 ± 0.308 μm and 6.936 ± 0.207 μm.) With this constant dr/dt, we infer that the reaction occurs primarily at the droplet surface. Were aqueous reactions the case, dr/dt would increase linearly with r_0, and the dr/dt data at ~ 7 μm would instead be clustered around 0.02 nm s^{-1}.

In the following, we normalize the sulfate formation rate with SO$_2$ concentration and droplet surface area, per the expression of reactive uptake coefficient Γ_{SO_2}:[26]

$$\Gamma_{SO_2} = \frac{dS(VI)/dt}{Z} \quad (4.1)$$

and

$$Z = \frac{1}{4}\sqrt{\frac{8RT}{\pi M_{SO_2}}}A[SO_{2(g)}]. \quad (4.2)$$

Here, Z is the collision efficiency between SO$_2$ molecules and droplet (unit, mol s^{-1}); the parameters R, T, M_{SO_2}, A, and $[SO_{2(g)}]$ are gas constant (J mol^{-1} K^{-1}), temperature (K^{-1}), SO$_2$ molecular weight (kg mol^{-1}), and droplet initial surface area (m^2), and SO$_2$ gas concentration (mol m$_{air}^{-3}$), respectively.

3.3 Influence of metal concentration

Not all Fe(III) in aerosol water are soluble. The soluble Fe(III) ions include $FeOH^{2+}$, $Fe(OH)_2^+$, and $Fe_2(OH)_2^{4+}$; their concentration in dilute solution might be estimated per the precipitation equilibrium relationship. But it remains unclear whether such a relationship still provides accurate predictions in aerosol water at the non-ideal, high-ionic-strength condition. Here, we empirically measured the reaction rate at changing concentrations of total Fe(III), including both soluble and insoluble Fe(III). In these experiments, droplet pH was maintained at ~ 5; ambient RH, at $\sim 60\%$. The molar fraction of total Fe(III) in droplet solute varied between 0.0001% and 0.1% (correspondingly, the total Fe(III) concentration varied between ~ 6.2 μM and ~ 6.2 mM.)

The results are shown in Fig. 3. Although the total Fe(III) varied across three orders of magnitude, the reaction rate at pH ≈ 5 remains a constant. This constant reaction rate indicates that most of the Fe(III) in droplets was insoluble. Such an observation of excessive total Fe(III) agrees with traditional kinetic studies. For example, Martin et al.[31] found that, at pH $\approx$ 5, the first-order rate coefficient of Fe(III)-catalyzed oxidation of aqueous S(IV) is also independent of Fe(III) concentration. In polluted air, the Fe(III) concentration is about 18 ng m$_{air}^{-3}$, and the aerosol water content is about 300 μg m$_{air}^{-3}$.[20] These conditions suggest that the total Fe(III) molarity in aerosol water is ~ 1 mM (dotted line in Fig. 3), far beyond the solubility limit. Therefore, one may assume that the reaction kinetics at fixed pH conditions is zeroth order in the total airborne Fe(III).
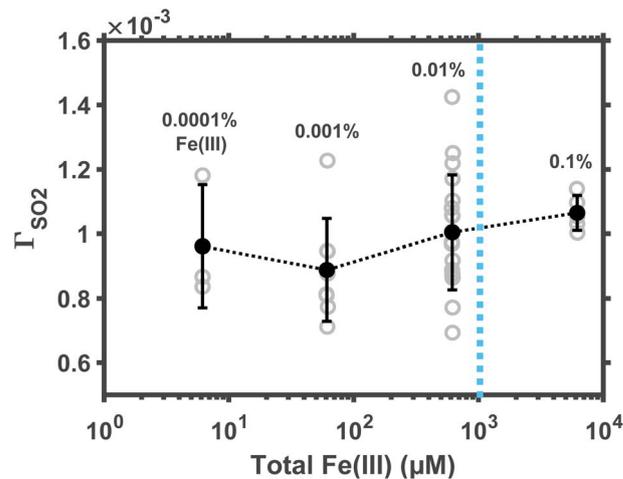

Fig. 3 Reaction rate is independent of the total Fe(III) concentration in microdroplets. The gray circle represents the reactive uptake coefficient Γ_{SO_2} data obtained from each experiment run. The black circle represents the mean Γ_{SO_2} values of the data in each bin, and the error bar represents one standard deviation. The vertical dotted line indicates the typical value of total Fe(III) molarity in aerosols at haze conditions. The droplet pH was maintained at ~ 5; the ambient RH, at $\sim 60\%$.

3.4 Influences of ambient humidity

We next investigate the influence of ambient humidity on reaction rate. In these experiments, the SO$_2$ was maintained at 25 ppb; Fe(III) molar fraction, at 0.01%. Ambient RH varied among 60, 70, and 80%. The results are plotted in Fig. 4. As RH decreases from 80 to 60%, the mean reaction rate increases by a factor of ~ 2. The faster reaction at lower RH conditions may arise from the kinetic salt effect. When RH decreases, droplet water becomes more concentrated, and droplet ionic strength I
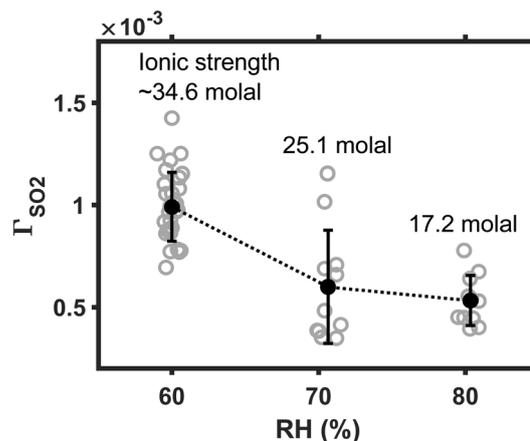

Fig. 4 The reaction rate decreases as ambient relative humidity (RH) increases. The gray circle represents the reactive uptake coefficient Γ_{SO_2} data obtained from each experiment run. The black circle represents the mean Γ_{SO_2} values of the data in each bin, and the error bar represents one standard deviation. The droplet pH was maintained at ~ 5; Fe(III) molar fraction, 0.01%.

increases. (For example, ESI Fig. S2† shows that the I of ammonium sulfate droplet increases from ~17 to 35 mol, as the ambient RH decreases from 80 to 60%.) Reactions are accelerated at the high I condition if the rate-limiting step of the reaction involves an interaction between charge neutral molecules and ions[1,26,32] here, the neutral SO_2 molecules and the $Fe(III)$ ions. This positive kinetic salt effect also indicates that SO_2 is directly converted at the droplet surface, without an *a priori* dissolution and dissociation.[1] For example, SO_2 and O_2 may react with $Fe(III)$ at droplet surface, producing $Fe(II)$ and SO_5^- radicals. Instead, if the SO_2 were first dissolved and dissociated into $S(IV)$ ions, then the rate-limiting step would involve an interaction between $S(IV)$ ions and $Fe(III)$ ions. Such ion–ion reaction would be inhibited when I is large.[17] One may refer to Angle *et al.*'s recent kinetic study[17] for such a slower TMI-catalyzed $S(IV)$ oxidation at higher I conditions.

The faster reaction rate at lower RH conditions is unlikely due to the enrichment effect (*i.e.*, droplet solvent evaporates, the aqueous reactant is concentrated, and the reaction is accelerated.) We find that this explanation is not very compelling, because when the SO_2 molecules are directly converted at the aerosol surface, their availability is unaffected by the enrichment of the aqueous phase. The $Fe(III)$ catalysts do exist in the aqueous phase. But, when the total $Fe(III)$ concentration is much greater than the solubility limit, the actual concentration of soluble $Fe(III)$ is unlikely to be affected by the enrichment of droplet water either.

3.5 Influence of Fe(III)/S(VI) coexisting time

The aqueous $Fe(III)$-catalyzed $S(IV)$ conversion is self-inhibiting because the reaction product $S(VI)$ is an effective complexation agent to the $Fe(III)$ catalysts.[17,24] Martin and Hill[24] reported that the $Fe(III)$-catalyzed reaction in bulk solution decelerates significantly when the $S(VI)$ concentration increases from a μM to a mM level. Here, we investigate the influence of $Fe(III)/S(VI)$ coexisting time on the heterogeneous reaction rate. In this part of experiment, we aged the AS/IS mixture solutions for 12, 36, or 48 hours before nebulizing them into aerosols. The reaction rate in the droplets made from aged solutions was then compared with that in the droplets made from the fresh solution. The SO_2 was maintained at 25 ppb; $Fe(III)$ molar fraction, at 0.01%. Ambient RH, at 60%. Fig. 5 plots the Γ_{SO_2} as a function of the $Fe(III)/S(VI)$ coexisting time. The reaction rate decelerates by almost a decade, as the $Fe(III)/S(VI)$ coexisting time increased from 0 to 48 hours. This observation indicates that the $Fe(III)/S(VI)$ complexation is also a significant factor affecting the heterogeneous SO_2 conversion. The $Fe(III)$-catalyzed reaction may be a decade slower in real-world sulfate aerosols that have gone through an elongated aging process.

3.6 Comparing with other reaction mechanisms

Table 1 compares the kinetic data obtained in the present study with those reported in ref. 1, 26 and 31. Per our present study, the $Fe(III)$-catalyzed SO_2 oxidation occurs primarily at aerosol surface. At room temperature and a pH ~5 condition, such a reaction exhibits Γ_{SO_2} on the order of 10^{-4}. This reaction rate
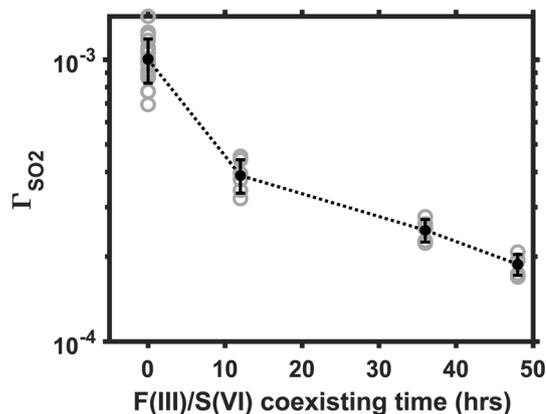

Fig. 5 Reaction rate decreases as the $Fe(III)/S(VI)$ coexisting time increases. The coexisting time refers to how long the AS/IS mixture solution was aged before being nebulized into aerosols. The gray circle represents the reactive uptake coefficient Γ_{SO_2} data obtained from each experiment run. The black circle represents the mean Γ_{SO_2} values of the data in each bin, and the error bar represents one standard deviation. The droplet pH was maintained at ~5; the ambient RH, at ~60%; $Fe(III)$ molar fraction, at 0.01%.

is 2–3 decades faster than what the solution chemistry predicts. For example, Martin *et al.*[31] reported that the $Fe(III)$-catalyzed $S(IV)$ oxidation in bulk solution at pH 5.0 has a first-order rate coefficient of ~10^{-3} s^{-1}. This rate coefficient corresponds to a Γ_{SO_2} of ~1.7×10^{-6} for the heterogeneous reaction inside the droplets with a ~10 μm radius (refer to Table 1 footnotes for details of calculation).

The much faster reaction rate observed in our present study is not an experimental artefact. Previously, Chen *et al.*[26] used the AOT to measure the uncatalyzed SO_2 oxidation rate in levitated droplets. In that study, we conducted the experiment by using the same AOT apparatus and the same ammonium sulfate chemicals, but we did not intentionally add any $Fe(III)$ to the droplets. At such conditions, the reaction at pH ~5.0 exhibited a Γ_{SO_2} on the orders of 10^{-7} to 10^{-6}. This comparison indicates that the 2-to-3-decade faster reaction observed here is due to our intentional addition of $Fe(III)$ to droplet water. In other words, if such faster kinetics were a systematic artefact of the AOT apparatus, Chen *et al.* would also observe a Γ_{SO_2} on the order of 10^{-4} for the uncatalyzed reactions.

One should also note that the Γ_{SO_2} on the order of 10^{-4} to 10^{-3} is even greater than what is needed to explain the missing sulfate in haze events. Such an observation indicates that the $Fe(III)$-catalyzed heterogeneous SO_2 oxidation in the atmosphere is not as fast as that in the laboratory aerosols, particularly those freshly-made ones. As we discussed earlier, the catalytic capability of $Fe(III)$ is impaired if $Fe(III)$ and $S(VI)$ coexists for a long time. On the other hand, recent studies proposed that a strong electric field exists at the air–water interface, triggering a spontaneous conversion of some OH^- ions at droplet surface into OH radicals and free electron.[33,34] Such unique environment at air–water interface may also alter the kinetics of redox reactions.

Table 1 Kinetics of heterogeneous SO_2 oxidation at room temperature

References	Catalysts	Reaction location	Conditions	Uptake coef.
The present study	Fe(III)	Aerosol surface	pH 5; 60% RH; incipient aerosols	$9.9(\pm1.7) \times 10^{-4}$
			pH 5; 80% RH; incipient aerosols	$5.3(\pm1.2) \times 10^{-4}$
			pH 5; 60% RH; aged aerosols	$1.4(\pm0.2) \times 10^{-4}$
Martin et al. (1991)	Fe(III)	Bulk solution[a]	pH 5; $r = 10$ μm (assumed)	$\sim1.7 \times 10^{-6}$
Chen et al. (2022)	Uncatalyzed	Aerosol surface[b]	pH 3.5–5.5; 60% RH	$\sim4.9 \times 10^{-7}$
			pH 3.5–5.5; 80% RH	$\sim8.1 \times 10^{-8}$
		Aerosol interior	pH 5; 60% RH; $r = 10$ μm (assumed)	$\sim6.6 \times 10^{-6}$
			pH 5; 80% RH; $r = 10$ μm (assumed)	$\sim5.5 \times 10^{-7}$
Wang et al. (2021)	Mn(II)	Aerosol surface[c]	pH 4–5; >80% RH; 0.81% Mn(II)	$\sim1.6 \times 10^{-4}$
			pH 4–5; >80% RH; 5.54% Mn(II)	$\sim7.1 \times 10^{-4}$

[a] Martin et al.[31] measured the rate of Fe(III)-catalyzed S(IV) oxidation in bulk solutions. They found that the first order rate coefficient k of this reaction is ca. 10^{-3} s^{-1} at pH 5.0 condition. One may estimate the corresponding uptake coefficient Γ_{SO_2} by using the eqn (4.1) in this paper. Specifically, rate per droplet is $dS(IV)/dt = (4/3)\pi r^3 k[S(IV)]$; the sulfite molarity $[S(IV)] = H_{SO_2}P_{SO_2}(1 + K_{1s}[H^+]^{-1} + K_{1s}K_{2s}[H^+]^{-2})$, where H_{SO_2} and P_{SO_2} respectively denote the Henry's law constant of SO_2 and SO_2 gas partial pressure. The K_{1s}, and K_{2s} respectively denote the first and second dissociation equilibrium constants of sulfite hydrate. Droplet radius r was assumed to be 10 μm matching our experimental condition. The P_{SO_2} is trivial and can take any arbitrary value. [b] Chen et al.[26] measured the uncatalyzed SO_2 oxidation rate in levitated aerosol microdroplets. The Γ_{SO_2} was calculated with eqn (5) and (8) in their paper. [c] Wang et al.[1] measured the Mn(II)-catalyzed SO_2 oxidation rate by using a smoke chamber. The Γ_{SO_2} was calculated with the dataset shown in the Fig. 1b in their paper.

4 Conclusion

In this work, we directly measured Fe(III)-catalyzed SO_2 conversion inside optically levitated microdroplets. We show that aerosol optical tweezers – coupled with cavity-enhanced Raman spectroscopy – can be utilized to determine the rate of heterogeneous reactions between SO_2 gas and microdroplets. Our findings show that the rate of Fe(III)-catalyzed SO_2 oxidation is first order in SO_2 concentration. During the heterogeneous reaction, the droplet growth rate is independent of the droplet initial radius, indicating that the sulfate production rate (per droplet) is proportional to the droplet surface area. Such a surface scaling law in turn suggests that the heterogeneous reaction occurs primarily at the air–water interface. The reaction rate is faster at lower RH conditions, possibly owing to a positive kinetic salt effect for ion–molecule reactions. The reaction rate at pH $\sim$ 5 remains constant despite the total Fe(III) molar fraction varies across three decades, indicating that most Fe(III) is insoluble. This excessive Fe(III) condition also holds valid for real-world aerosols in polluted air. The reaction rate decelerates nearly one decade as the Fe(III)/S(VI) coexists for two days, indicating that the contribution of the Fe(III)-catalyzed reaction to sulfate may significantly diminish in aged aerosols.

Author contributions

P. L. and Y. Z. designed the research; X. C. and Z. C. performed the experiments; P. L. performed the theoretical calculations; P. L. and X. C. wrote the first draft of the manuscript; and all of the authors analyzed the data and contributed to revising the manuscript.

Conflicts of interest

There are no conflicts to declare.

Acknowledgements

References

1 W. Wang, M. Liu, Y. Song and M. Ge, Sulfate formation is dominated by manganese-catalyzed oxidation of SO_2 on aerosol surfaces during haze events, *Nat. Commun.*, 2021, **12**, 1–10.

2 J. P. D. Abbatt and O. Mohler, Solid ammonium sulfate aerosols as ice nuclei: A pathway for cirrus cloud formation, *Science*, 2006, **313**, 1770–1773.

3 C. A. Pope and G. D. Thurston, Lung cancer, cardiopulmonary mortality, and long-term exposure to fine particulate air pollution, *JAMA*, 2002, **287**, 1132–1141.

4 H. He and J. Hao, Mineral dust and NO_x promote the conversion of SO_2 to sulfate in heavy pollution days, *Sci. Rep.*, 2014, **4**, 4172.

5 F. Yan, W. Chen and X. Wang, Stabilization for the secondary species contribution to $PM_{2.5}$ in the Pearl River Delta (PRD) over the past decade, China: A meta-analysis, *Atmos. Environ.*, 2020, **242**, 117817.

6 D. Shang, J. Peng, S. Guo, Z. Wu and M. Hu, Secondary aerosol formation in winter haze over the Beijing-Tianjin-Hebei Region, China, *Front. Environ. Sci. Eng.*, 2021, **15**, 1–13.

7 X. Li, B. Zhao, W. Zhou and J. Jiang, Responses of gaseous sulfuric acid and particulate sulfate to reduced SO_2 concentration: a perspective from long-term measurements in Beijing, *Sci. Total Environ.*, 2020, **721**, 137700.

8 P. Kasibhatla, W. L. Chameides and J. S. John, A three-dimensional global model investigation of seasonal variations in the atmospheric burden of anthropogenic sulfate aerosols, *J. Geophys. Res.: Atmos.*, 1997, **102**, 3737–3759.

9 W. R. Stockwell and J. G. Calvert, The mechanism of the HO-SO_2 reaction, *Atmos. Environ.*, 1983, **17**, 2231–2235.

10 R. L. Mauldin, T. Berndt and M. Kulmala, A new atmospherically relevant oxidant of sulphur dioxide, *Nature*, 2012, **488**, 193–196.

11 T. Liu, A. W. H. Chan and J. P. D. Abbatt, Multiphase oxidation of sulfur dioxide in aerosol particles: Implications for sulfate formation in polluted environments, *Environ. Sci. Technol.*, 2021, **55**, 4227–4242.

12 J. H. Seinfeld and S. N. Pandis, *Atmospheric Chemistry and Physics: From Air Pollution to Climate Change*, John Wiley & Sons, 3rd edn, 2016.

13 Y. Wang, Q. Zhang and Y. Xie, Enhanced sulfate formation during China's severe winter haze episode in January 2013 missing from current models, *J. Geophys. Res.: Atmos.*, 2014, **119**, 10425–10440.

14 G. Li, H. Su and Y. Cheng, Multiphase chemistry experiment in fogs and aerosols in the North China Plain (McFAN): integrated analysis and intensive winter campaign 2018, *Faraday Discuss.*, 2021, **226**, 207–222.

15 X. Wang, Y. Lei, T. Liu and K. He, A unit-based emission inventory of SO_2, NO_x and PM for the Chinese iron and steel industry from 2010 to 2015, *Sci. Total Environ.*, 2019, **676**, 18–30.

16 H. Zhang, Y. Xu and L. Jia, A chamber study of catalytic oxidation of SO_2 by Mn^{2+}/Fe^{3+} in aerosol water, *Atmos. Environ.*, 2021, **245**, 118019.

17 K. J. Angle, E. E. Neal and V. H. Grassian, Enhanced rates of transition-metal-ion-catalyzed oxidation of S(IV) in aqueous aerosols: Insights into sulfate aerosol formation in the atmosphere, *Environ. Sci. Technol.*, 2021, **55**, 10291–10299.

18 M. Gen, R. Zhang, D. D. Huang, Y. Li and C. K. Chan, Heterogeneous oxidation of SO_2 in sulfate production during nitrate photolysis at 300 nm: Effect of pH, relative humidity, irradiation intensity, and the presence of organic compounds, *Environ. Sci. Technol.*, 2019, **53**, 8757–8766.

19 Y. W. Chen and J. P. Burrows, Contribution of the gas-phase reaction between hydroxyl radical and sulfur dioxide to the sulfate aerosol over West Pacific, *Atmos. Chem. Phys.*, 2021, **2021**, 1–29.

20 Y. Cheng, Z. Wang and H. Su, Reactive nitrogen chemistry in aerosol water as a source of sulfate during haze events in China, *Sci. Adv.*, 2016, **2**, e1601530.

21 T. Liu, S. L. Clegg and J. P. D. Abbatt, Fast oxidation of sulfur dioxide by hydrogen peroxide in deliquesced aerosol particles, *Proc. Natl. Acad. Sci. U. S. A.*, 2020, **117**, 1354–1359.

22 J. Gao, G. Shi and A. Nenes, Targeting atmospheric oxidants can better reduce sulfate aerosol in China: H_2O_2 aqueous oxidation pathway dominates sulfate formation in haze, *Environ. Sci. Technol.*, 2022, **56**, 10608–10618.

23 T. Wang, M. Liu, Y. Song, M. Hu and T. Zhu, Sulfate formation apportionment during winter haze events in North China, *Environ. Sci. Technol.*, 2022, **56**, 7771–7778.

24 L. R. Martin and M. W. Hill, The iron catalyzed oxidation of sulfur: reconciliation of the literature rates, *Atmos. Environ.*, 1967, **21**, 1487–1490.

25 L. R. Martin and T. W. Good, Catalyzed oxidation of sulfur dioxide in solution: the iron-manganese synergism, *Atmos. Environ., Part A*, 1991, **25**, 2395–2399.

26 Z. Chen, P. Liu, W. Wang, X. Cao, Y. Zhang and M. Ge, Rapid sulfate formation *via* uncatalyzed autoxidation of sulfur dioxide in aerosol microdroplets, *Environ. Sci. Technol.*, 2022, **56**, 7637–7646.

27 R. Symes, R. M. Sayer and J. P. Reid, Cavity enhanced droplet spectroscopy: principles, perspectives and prospects, *Phys. Chem. Chem. Phys.*, 2004, **6**, 474–487.

28 T. C. Preston and J. P. Reid, Accurate and efficient determination of the radius, refractive index, and dispersion of weakly absorbing spherical particle using whispering gallery modes, *J. Opt. Soc. Am. B*, 2013, **30**, 2113–2122.

29 A. S. Wexler and S. L. Clegg, Atmospheric aerosol models for systems including the ions H^+, NH_4^+, Na^+, SO_4^{2-}, NO_3^-, Cl^-, Br^-, and H_2O, *J. Geophys. Res.: Atmos.*, 2002, **107**, 4207.

30 J. H. Seinfeld and S. N. Pandis, *Atmospheric Chemistry and Physics: From Air Pollution to Climate Change, Atmospheric Chemistry and Physics of Air Pollution*, 3rd edn, 2016.

31 L. R. Martin, M. W. Hill, A. F. Tai and T. W. Good, The iron catalyzed oxidation of sulfur(IV) in aqueous solution: differing effects of organics at high and low pH, *J. Geophys. Res.: Atmos.*, 1991, **96**, 3085–3097.

32 H. Herrmann, Kinetics of aqueous phase reactions relevant for atmospheric chemistry, *Chem. Rev.*, 2003, **103**, 4691–4716.

33 J. P. Heindel, H. Hao, R. A. LaCour and T. Head-Gordon, Spontaneous formation of hydrogen peroxide in water microdroplets, *J. Phys. Chem. Lett.*, 2022, **13**, 10035–10041.

34 D. Xing and X. Zhang, Capture of hydroxyl radicals by hydronium cations in water microdroplets, *Angew. Chem.*, 2022, **61**, e202207587.